Astron. Astrophys. 273, 293–303 (1993)

ASTRONOMY AND ASTROPHYSICS

The chromospheric temperature rise in solar magnetic flux tubes

J.H.M.J. Bruls[1] **and S.K. Solanki**[2]

[1] Sterrekundig Instituut, Postbus 80 000, NL–3508 TA Utrecht, The Netherlands
[2] Institut für Astronomie, ETH-Zentrum, CH–8092 Zürich, Switzerland

Received September 17, 1992; accepted January 2, 1993

Abstract. We set constraints on the location and steepness of the chromospheric temperature rise in solar magnetic flux tubes by synthesizing Stokes V profiles in non-local thermodynamic equilibrium (NLTE) of a set of "clean" Fe I and Fe II lines of different strengths. We compute profiles for several flux-tube models of the magnetic features within solar network and plage. Comparison with observed V profiles indicates that both in network and plage the chromospheric temperature rise starts at larger optical depth within the flux tubes than in the surrounding non-magnetic atmosphere. The exact onset cannot be determined with the present set of lines because they cannot easily distinguish between the location and initial steepness of the temperature rise. Assuming a similar $T(\tau)$ gradient as in quiet-Sun models, the chromosphere sets in 200 – 300 km deeper in flux tubes than in the quiet Sun. The similarity between the plage and network results suggests that in the low chromosphere the heating per flux tube is almost independent of magnetic filling factor.

Key words: line: profiles – Sun: atmosphere – Sun: chromosphere – Sun: magnetic fields

1. Introduction

Empirical models of the solar chromosphere are required to guide theories of chromospheric heating. Single-component models (e.g. Vernazza et al. 1981) have been refined over many years, but the necessity of two-component, or even 2-D modeling has recently become increasingly clear (Ayres & Testerman 1981, Ayres et al. 1986, Solanki & Steiner 1990, Solanki et al. 1991). In such modeling, small-scale magnetic features are generally represented by flux tubes. Detailed empirical models of the photospheric layers of flux tubes have been formulated. Recent examples are those by Solanki (1986), Walton (1987), Keller et al. (1990) and Solanki & Brigljević (1992). However, empirical models of the chromosphere within flux tubes have a less sound basis. Only Ayres et al. (1986), using a purely two-component model, and Solanki et al. (1991), using a 2-D model, have attempted to constrain the temperature in the chromospheric layers of flux tubes. However, their analyses are based on unpolarized, Stokes I, profiles of the Ca II K line. Those allow for different interpretations, depending on the choice of filling factor and temperature of the external atmosphere. In this paper we attempt to extend semi-empirical modeling of the temperature stratification and magnetic field strength in magnetic elements of the solar photosphere to the low chromosphere using Stokes V profiles.

Empirical flux-tube models are generally based on a two-component or a simple 2-D approach, consisting of a magnetic flux tube with height-dependent area filling factor α and an ambient non-magnetic part covering the area outside the tube. Since present observations have insufficient spatial resolution to resolve single flux tubes, two-component modeling is required to derive parameters that pertain to the magnetic features alone.

So far, two-component modeling has generally involved fitting computed LTE (local thermodynamic equilibrium) Stokes V profiles to observed profiles of network and plage regions (Stenflo 1975, Solanki 1986, Keller et al. 1990). The presence of a chromospheric temperature rise, which is thought to be particularly pronounced in magnetic features (e.g. Chapman 1981, Ayres et al. 1986, Schrijver et al. 1989), cannot be revealed with LTE methods because they determine the excitation temperatures rather than the local electron temperature. NLTE computations are therefore needed to derive information about the chromospheric electron temperature stratification. NLTE calculations in flux tubes have been limited to either exploratory calculations (Stenholm & Stenflo 1977, 1978, Solanki & Steenbock 1988), or to fitting non-LTE Stokes I profiles to intensity data, i.e. without using polarization information (Solanki et al. 1991). So far, no empirical models based on NLTE computations of Stokes V profiles have been reported. We undertake such an analysis using the response of computed Stokes V profiles of Fe I and Fe II lines of different strength to chromospheric temperature variations as a guide to constrain flux-tube chromospheres.

Send offprint requests to: J.H.M.J. Bruls, currently at Institut für Astronomie, ETH-Zentrum, CH–8092 Zürich, Switzerland

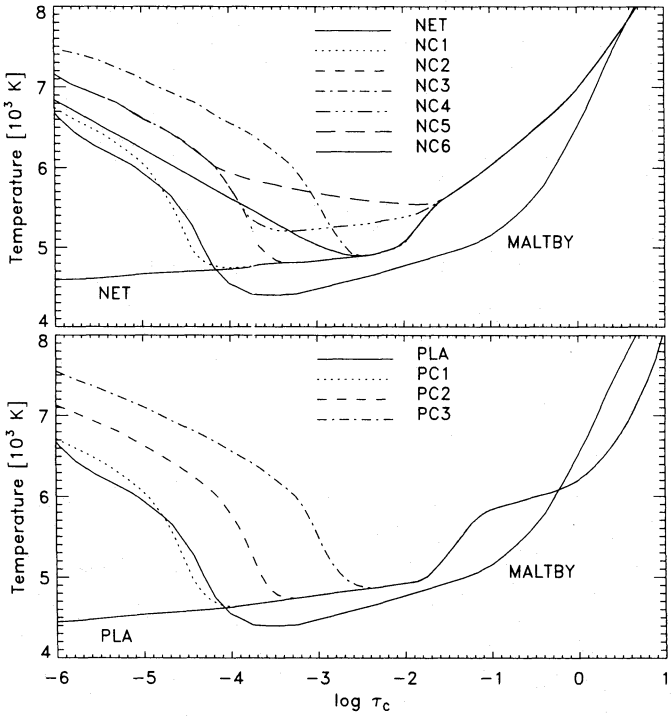

Fig. 1. Temperature versus continuum optical depth τ_c at 5000 Å for each flux-tube model. Top panel: network models; bottom panel: plage models. The models without chromospheric temperature rise (solid curves) are the NET model from Solanki (1986) and the PLA model from Solanki & Brigljević (1992). The other models were constructed by adding a chromosphere similar to the one of the Maltby et al. (1986) quiet-Sun model, at different heights and with different transition prescriptions

Table 1. Line data: wavelength λ, excitation energy $E_{\rm exc}$, oscillator strength $\log gf$, radiative broadening $\gamma_{\rm rad}$, γ_6 enhancement factor. Numbers in parentheses denote exponents: e.g. 1.12(4) means $1.12\ 10^4$. The first 18 lines are Fe I lines and the last six are Fe II lines

λ [Å]	$E_{\rm exc}$ [eV]	$\log gf$	$\gamma_{\rm rad}$ [s^{-1}]	γ_6 factor
5127.68	0.05	−6.06	1.12(4)	0.96
5247.06	0.09	−4.97	1.32(4)	0.97
5250.20	0.12	−4.96	7.30(3)	0.97
5405.77	0.99	−1.98	1.84(7)	1.11
5083.34	0.96	−3.00	2.18(7)	1.10
4798.73	1.61	−4.25	1.72(8)	1.20
5145.09	2.20	−3.26	1.39(8)	1.29
5253.02	2.28	−3.90	3.17(8)	1.30
4848.88	2.28	−3.43	4.78(8)	1.30
4794.35	2.42	−4.04	1.00(9)	1.34
5232.94	2.94	−0.02	3.18(8)	1.84
5217.39	3.21	−1.00	2.36(8)	2.11
4907.73	3.43	−1.88	3.14(8)	2.33
4809.94	3.57	−2.65	9.35(8)	2.47
5242.49	3.63	−1.05	3.26(8)	2.50
4799.06	4.28	−2.81	5.14(8)	2.50
5383.37	4.31	0.48	3.49(8)	2.50
5412.79	4.43	−1.87	4.86(8)	2.50
5132.67	2.81	−4.23	2.94(8)	2.50
5256.94	2.89	−4.32	2.86(8)	2.50
4923.92	2.89	−1.43	2.50(8)	2.50
5414.07	3.22	−3.78	2.70(8)	2.50
5197.58	3.23	−2.31	2.44(8)	2.50
5325.55	3.22	−3.38	2.56(8)	2.50

2. Computational aspects and observational data

2.1. Flux-tube models

We use cylindrically symmetric two-component atmospheric models. These models consist of a magnetic flux tube that expands radially with height, embedded in a non-magnetic atmosphere which we represent by a quiet-Sun model (Maltby et al. 1986). The radial expansion of the flux tube is described by the "thin-tube" approximation, which is the zeroth order solution of the magnetohydrostatic equilibrium equations: within the flux tube all radial derivatives of state parameters are set to zero (e.g. Defouw 1976, Schüssler 1986). Following, e.g., Solanki (1986) and Keller et al. (1990) we model flux tubes in active region plages and the quiet network separately. The magnetic areas of the solar atmosphere are assumed to contain numerous flux tubes; the discriminating difference between network and plages is formed by their magnetic filling factors, which at $\tau_c = 1$ range from a few percent of the area in the network to a few tens of percents in active region plages, and by the indication that the photospheric flux-tube temperature decreases with increasing filling factor (Solanki 1990). Possible size differences between the flux tubes in network and plages (Solanki & Brigljević 1992 and references therein) do not enter directly into our analysis, since it is restricted to regions close to disk center. Such size differences are taken into account indirectly through the dependence of the magnetic filling factor (i.e. the fractional area at a given height that is covered by magnetic fields) on the thermal stratification.

The network flux-tube models used here (Fig. 1) are based on the NET model of Solanki (1986), which was obtained by fitting several hundred Fe I and Fe II Stokes V profiles assuming LTE. The flux-tube chromospheres are ad-hoc extensions, differing only in location and initial gradient of the temperature rise. The network models NC1-3 were constructed by combining the NET flux tube model with a lower chromosphere similar to the one of the Maltby et al. (1986) quiet-Sun model; they differ only in the optical depth τ_{5000} at which the chromospheric temperature rise begins. The models NC4 and NC5 were constructed from NC2, but do not share the sudden temperature drop in the upper photosphere which is perhaps an artefact of the LTE modeling on which NET is based. NC6 is discussed in Sect. 4 below. A set of plage models (Fig. 1 bottom panel) was similarly constructed from the PLA model of Solanki & Brigljević (1992), which is an improved version of the plage model of Solanki (1986). Note that all models satisfy the constraints on $T(\tau_{5000} = 1)$ set by observed C I lines (Solanki & Brigljević 1992). This is an important property since the computations of Solanki & Steenbock (1988) have shown that, for a

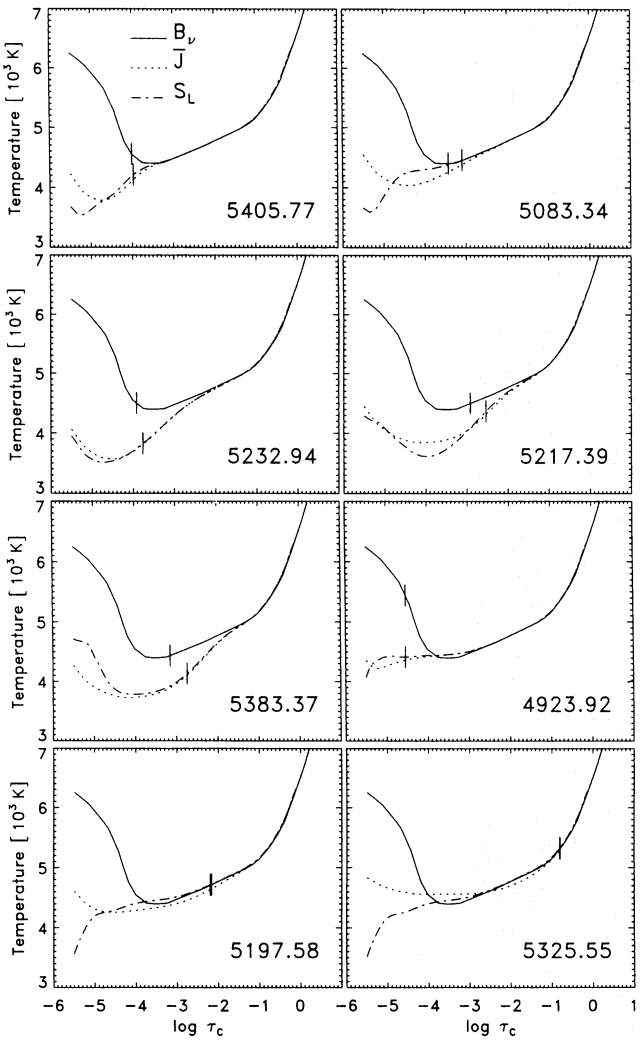

Fig. 2. Quiet-Sun line formation properties: line source functions S_L and line averaged radiation fields $\overline{J}$. Tickmarks indicate the $\tau_{\nu_0} = 1$ locations for LTE (on the B_ν curves) and NLTE line formation (on the S_L curves); the NLTE marks are the deeper ones. The lines 4923.92, 5197.58 and 5325.55 Å are Fe II lines

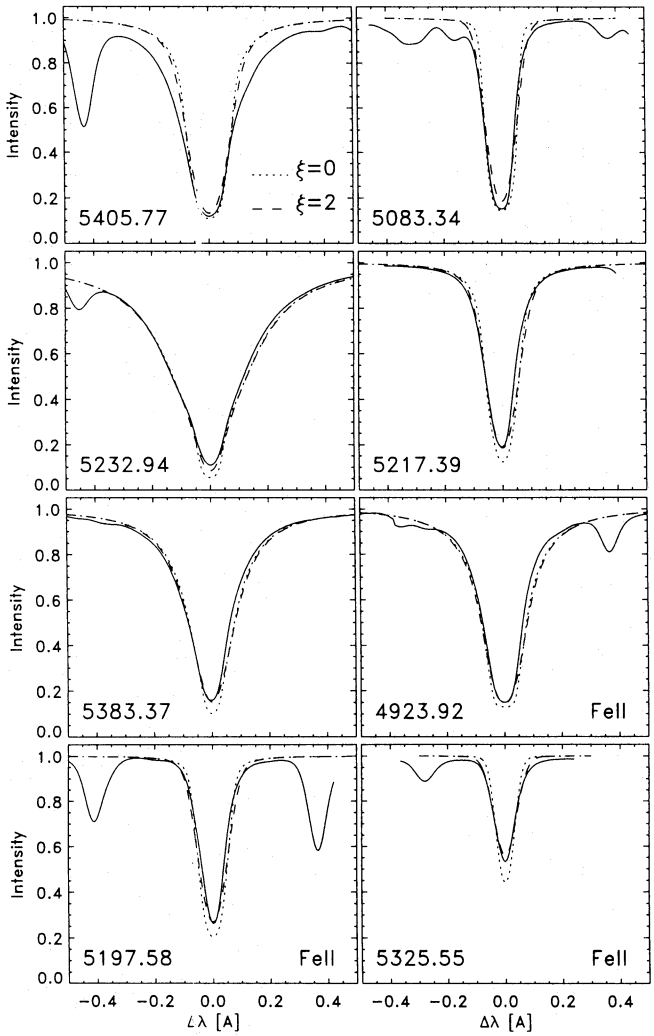

Fig. 3. Quiet-Sun line profiles; intensity relative to continuum. Solid curves: observed profiles. Dotted curves: computed profiles. Dashed curves: computed profiles convolved with a 2 km s^{-1} macroturbulence velocity. The dotted and dashed profiles give an impression of extent of the smearing required to fit the observed profiles

given $T(\tau)$ in the line-forming layers, the departures from LTE in Fe I lines are determined mainly by the continuous radiation field; the same holds for Fe II lines (cf. Rutten 1988).

2.2. *Observational data*

A set of 18 Fe I and 6 Fe II lines (Table 1) provides our diagnostics. The lines were selected from a larger sample observed in 1979 with the Kitt Peak McMath telescope, using the Fourier Transfrom Spectrometer (FTS) to record intensity and circular polarization Stokes V spectra simultaneously (see Stenflo et al. 1984 for details concerning the observations). The spatial resolution of the observations is low, so that the observed Stokes I line profiles are of mixed magnetic and non-magnetic origin. Additionally, the long exposure time averaged the effect of wave-like phenomena, in particular the 5-minute oscillation. However, the spectral resolution and the signal-to-noise ratio are high, so that even small distortions of the line profiles are solar in origin. We compare our synthetic profiles with two FTS spectra, one obtained in a solar network region (small magnetic filling factor), the other in an active region plage (larger filling factor).

Our choice of lines reconciles several criteria: (*i*)—The lines should cover a large area in the equivalent width–excitation energy (W_λ, $E_{\rm exc}$)-plane, so that different heights in the atmosphere and different temperature sensitivities are sampled. (*ii*)—The lines should be as clean (unblended) as possible. (*iii*)—All lines should come from the same FTS scan to ensure that they originate from the same area on the Sun and were taken synchronously; this limits the wavelength coverage. (*iv*)—The lines should have reasonable magnetic splitting, preferentially with Landé factors $g_{\rm eff} \geq 1$, to provide sufficient signal to noise in Stokes V. (*v*)—LS coupling should be a good description for all

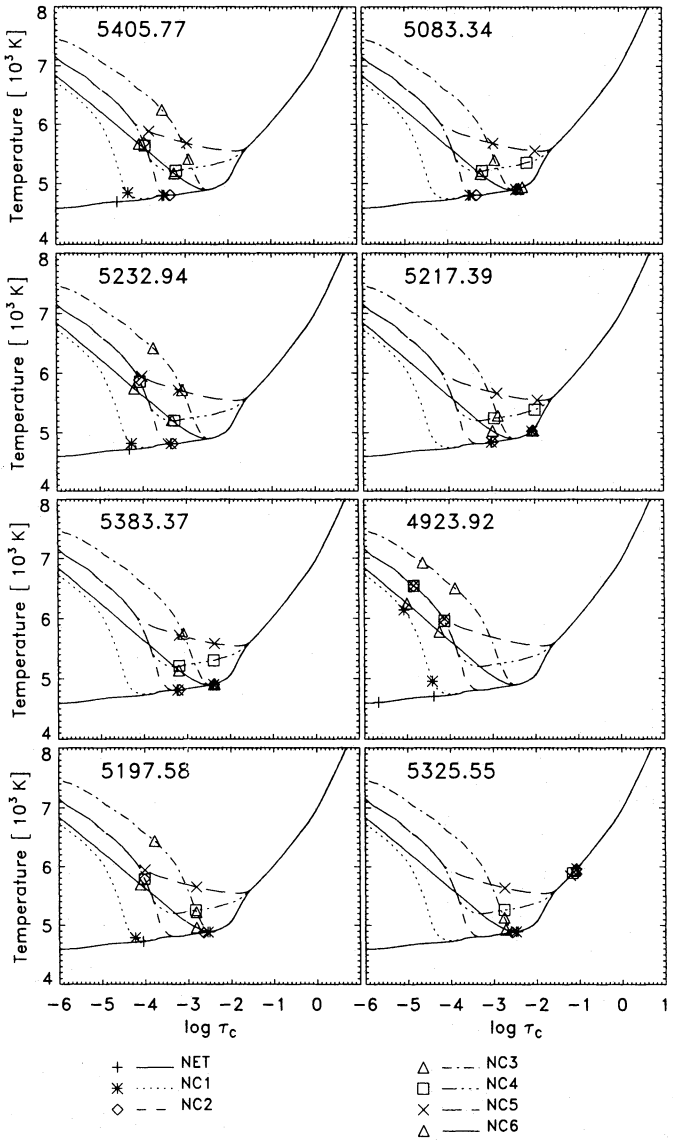

Fig. 4. Network model formation heights. The symbols represent the locations of the $\tau_{\nu_0} = 0.1$ and $\tau_{\nu_0} = 1$ points along the central line of sight of each flux-tube model for the eight strongest lines, ignoring Zeeman splitting

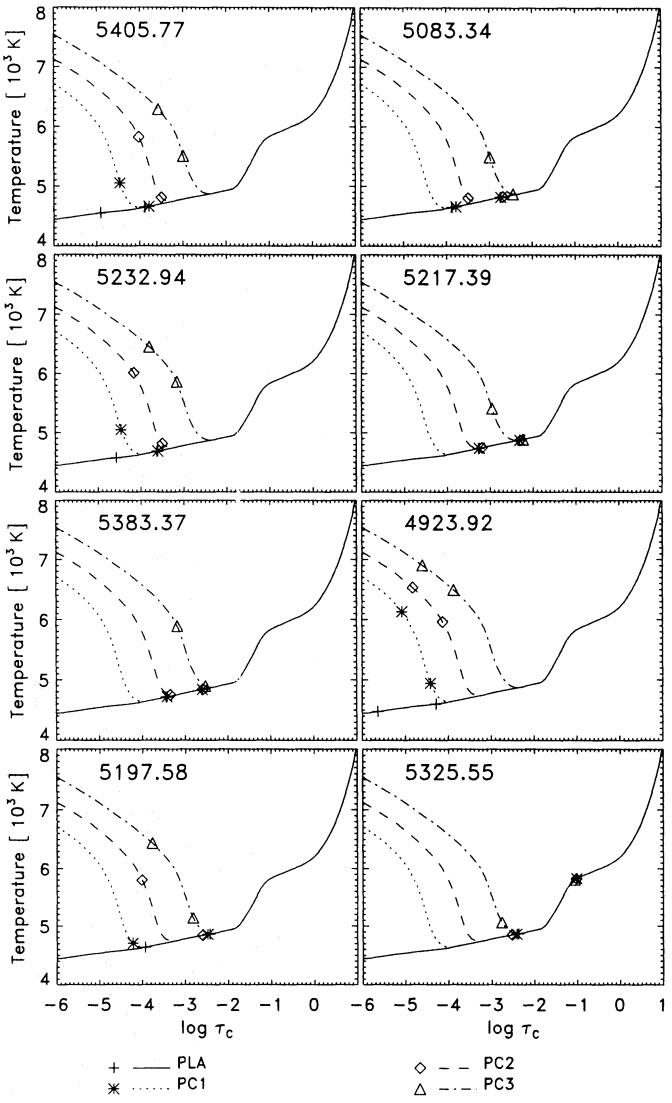

Fig. 5. Plage model formation heights: $\tau_{\nu_0} = 0.1$ and $\tau_{\nu_0} = 1$ points on the central line of sight of each flux-tube model for the unsplit line profiles

lines, since the Stokes profile synthesis code (Rees et al. 1989) used here relies on that approximation. (*vi*)—All lines should be present in, or easily added to, the 100-level model iron atom constructed by Watanabe & Steenbock (1986).

2.3. Radiative transfer and model atom

The NLTE statistical equilibrium calculations were performed in one-dimensional fashion for 10 representative vertical lines of sight through each two-component atmosphere at different distances from the flux-tube center (see Solanki & Roberts 1992 for a description). Each line of sight is treated as an infinitely extending plane-parallel atmosphere. Lateral radiative transfer is neglected in this formalism, although it may be important for small structures in the solar photosphere (Stenholm & Stenflo 1977, 1978, Mihalas et al. 1978, Jones & Skumanich 1980, Owocki & Auer 1980). This neglect may overestimate lateral variations since no smoothing is incorporated; in particular, Nordlund (1991) shows that for granular temperature variations the actual angle-averaged radiation field is considerably smoothed in the upper atmosphere due to lateral radiative transport through scattering.

The initial statistical equilibrium computation employs version 2.0 of the Carlsson (1986) code MULTI and produces non-magnetic NLTE line source functions. The magnetic field is neglected in these computations following the field-free approximation (Rees 1969), which is sufficiently accurate (Rees et al. 1989). Afterwards, the source functions are integrated for magnetically split line profiles using the Diagonal Element Lambda Operator (DELO) method of Rees et al. (1989) with the code de-

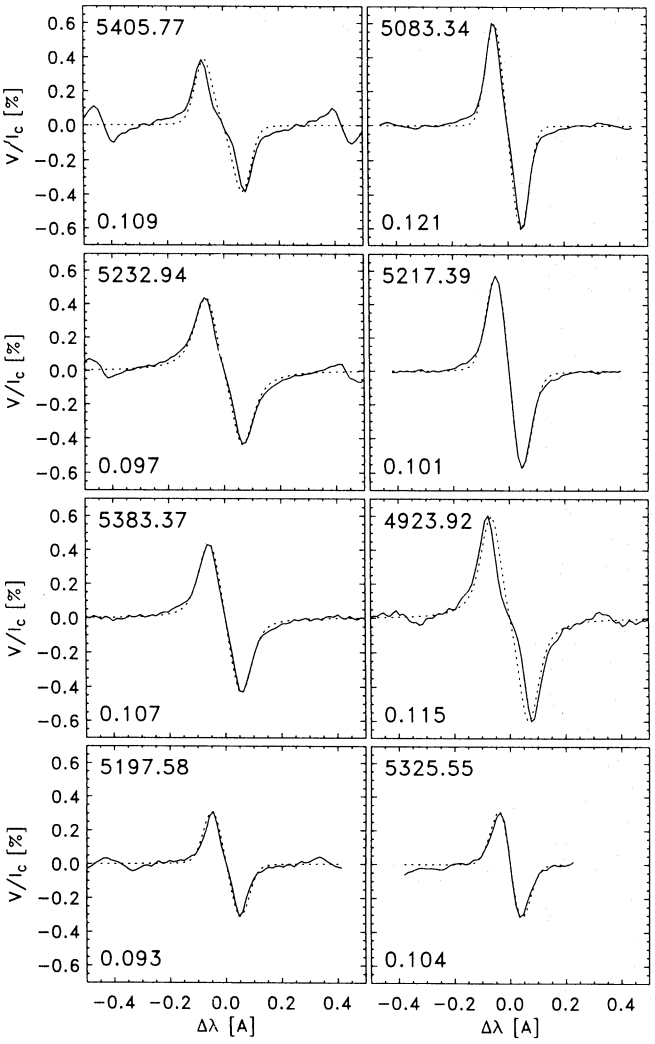

Fig. 6. Dotted curves: computed (scaled) Stokes V profiles for the NET model, after 2 km s^{-1} macroturbulent broadening. Solid lines: anti-symmetrized profiles observed in the network. The amplitude scaling factor is indicated in the lower left of each panel

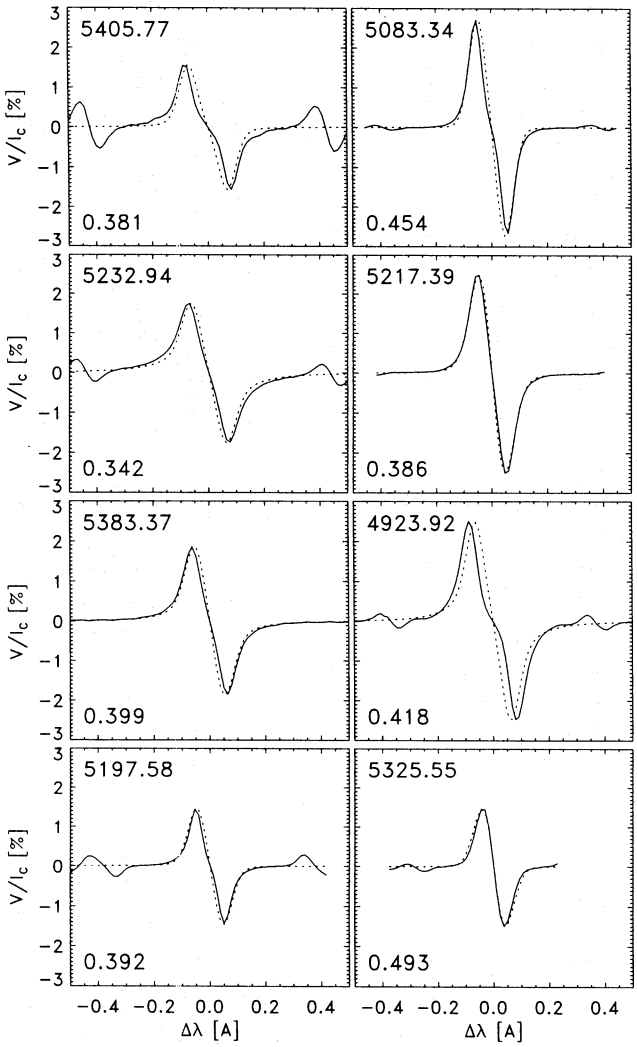

Fig. 7. Dotted curves: computed (scaled) Stokes V profiles for the PLA model. Solid lines: anti-symmetrized profiles observed in an active region plage

scribed by Murphy (1990) and Murphy & Rees (1990). Finally, the computed line profiles for all lines of sight are averaged with appropriate weights to represent a cylindrical flux-tube geometry embedded in a non-magnetic environment following Steiner & Pizzo (1989). This procedure is frequently called the 1.5-D approach.

The model atom employed in the statistical equilibrium computations is a modified version of the 100-level model atom presented by Watanabe & Steenbock (1986) and Gigas (1986). Only minor changes were necessary to incorporate all desired lines (Table 1), since the lines were selected subject to the presence of their upper and lower levels in this model. The oscillator strengths are from Thévenin (1989), who supplies a homogeneous list of empirical oscillator strengths based on the solar spectrum. His resulting oscillator strengths and abundance are slightly model dependent: for the Holweger & Müller (1974) quiet-Sun model, which closely resembles our Maltby et al. (1986) model, Thévenin recommends an abundance value of 7.61 on the log N_H = 12 scale. These oscillator strengths compare well with the experimental values tabulated by Fuhr et al. (1988). The electron collisional excitation cross sections specified in the 100-level atom of Gigas (1986) have been adopted. These cross sections are based on cool star line fits with rough assumptions, but represent the best available estimate in the literature. Neutral hydrogen collisional excitations have been neglected because they mainly act between close-lying levels, which already have nearly equal population departure coefficients as a result of the complex atomic structure with strong radiative coupling. The radiative line broadening is based on lifetime measurements by Assousa & Smith (1972), Klose (1971) and Corliss & Tech (1967).

Table 2. Formation heights in quiet-Sun atmosphere

λ [Å]	$\log \tau_{5000}$ @		h [km] @	
	$\tau_{\nu_0} = 0.1$	$\tau_{\nu_0} = 1$	$\tau_{\nu_0} = 0.1$	$\tau_{\nu_0} = 1$
5127.68	−1.75	−0.23	258	27
5247.06	−2.98	−1.73	430	254
5250.20	−2.95	−1.70	426	249
5405.77	−4.49	−3.86	680	549
5083.34	−3.86	−2.94	548	425
4798.73	−1.86	−0.43	273	53
5145.09	−2.27	−1.01	332	146
5253.02	−1.56	−0.24	228	28
4848.88	−1.96	−0.63	288	84
4794.35	−1.30	−0.08	190	8
5232.94	−4.41	−3.63	656	516
5217.39	−3.30	−2.38	472	348
4907.73	−2.25	−1.11	330	161
4809.94	−1.42	−0.19	208	21
5242.49	−2.88	−1.85	417	272
4799.06	−1.05	−0.01	152	0
5383.37	−3.42	−2.61	488	380
5412.79	−1.39	−0.23	204	26
5132.67	−1.53	−0.31	224	36
5256.94	−1.40	−0.23	205	27
4923.92	−5.12	−4.36	976	641
5414.07	−1.56	−0.36	229	44
5197.58	−3.96	−1.99	563	291
5325.55	−1.98	−0.66	291	90

2.4. Line broadening

Although inhomogeneities and oscillations in the solar atmosphere can probably account for the discrepancy between observed spatially-averaged line widths and one-dimensionally computed line widths (e.g. Nordlund 1984; Bruls & Rutten 1992), we have no other option but to invoke additional line broadening numerically by means of classical micro- and macroturbulence and Van der Waals broadening enhancements. Inside the magnetic flux tube we specify height-independent 1 km s^{-1} microturbulence, outside the tube we use the height-dependent values of the Maltby et al. (1986) quiet-Sun model. The Van der Waals broadening enhancements over the standard Unsöld (1955) values conform to the recipe of Simmons & Blackwell (1982), who suggest excitation dependent enhancement which we extrapolate to a maximum of 2.5. We use this maximum factor for higher-excitation Fe I lines as well as all Fe II lines. Macroturbulent broadening of up to 3 km s^{-1} is applied to the area-averaged line profiles to simulate oscillatory phenomena or other motions in the atmosphere.

3. Results

In this section we present computed line profiles and formation heights. Using the latter, we first select those lines that may display sensitivity to chromospheric state-parameter variations (Sect. 3.1). For these lines more detailed results are presented in Sect. 3.2.

3.1. Quiet-Sun results

Table 2 lists the location of the line center optical depths $\tau_{\nu_0} = 0.1$ and $\tau_{\nu_0} = 1$ for the complete set of lines, computed for the Maltby et al. (1986) quiet-Sun model atmosphere. Only five Fe I and two Fe II lines turn out to be sufficiently strong to be sensitive to model atmosphere changes above $\tau_{5000} = 10^{-2}$, which is required to discriminate between different chromospheric models. A third Fe II line is included with these seven lines to provide a photospheric reference that is not severely affected by NLTE ionization.

We assess the basic NLTE formation properties of the eight lines selected in Fig. 2, which displays the NLTE line source functions together with the Planck function and the profile-averaged angle-averaged radiation field $\overline{J}$. Tickmarks indicate the line center optical depth unity locations for LTE and NLTE line formation. The Fe I NLTE line source functions drop below their LTE values due to line photon losses. The Fe I NLTE line opacities are smaller than in LTE, resulting in deeper formation, due to superthermal ultraviolet radiation fields from below (cf. Rutten 1988). The Fe II lines have LTE opacities and line source functions. Only the Fe II 4923.92 Å line source function deviates significantly from LTE in the line center formation region. Similar NLTE departures occur for the network and plage models. The source function departures are larger for models with a deeper onset of the chromosphere whereas the opacity departures are the same because they are set already in the deep photosphere.

Figure 3 displays the reproduction of the quiet-Sun profiles of the eight lines. Macroturbulent broadening of order 2 km s^{-1} greatly improves the correspondence between the observed and computed profiles. The computed profiles fit the observed profiles quite satisfactorily, except for Fe I 5405.77 Å. In the $(W_\lambda, E_{\rm exc})$-plane this line is surrounded by lines Fe I 5083.34, 5217.39, 5383.37, and 5232.94 Å, which have comparable strengths and non-LTE effects but which are all reproduced well. If a strong unidentified blend, not originating from iron, were present (necessarily near line center, because of the symmetry), the semi-empirical analysis by Thévenin (1989) would have yielded an oscillator strength considerably larger than the Fuhr et al. (1988) value, which is not the case. The reason for this discrepancy is not clear.

3.2. NET and PLA results

In Figs. 4 and 5 we present formation heights along the ray corresponding to the axis of the the flux tube, in the form of $\tau_{\nu_0} = 0.1$ and $\tau_{\nu_0} = 1$ depths for the case without magnetic splitting. These depths approximately correspond to $\tau_{\nu_0} = 0.1$ and $\tau_{\nu_0} = 1$ for the magnetically split components of the lines.

Figures 6 and 7 display the observed (solid) and computed (dotted) Stokes V components. The observed profiles have been anti-symmetrized with respect to their zero-crossing wavelength, by means of simple averaging, in order to remove as far as possible the effects introduced by velocity gradients; this procedure also reduces the influence of noise and blends on the

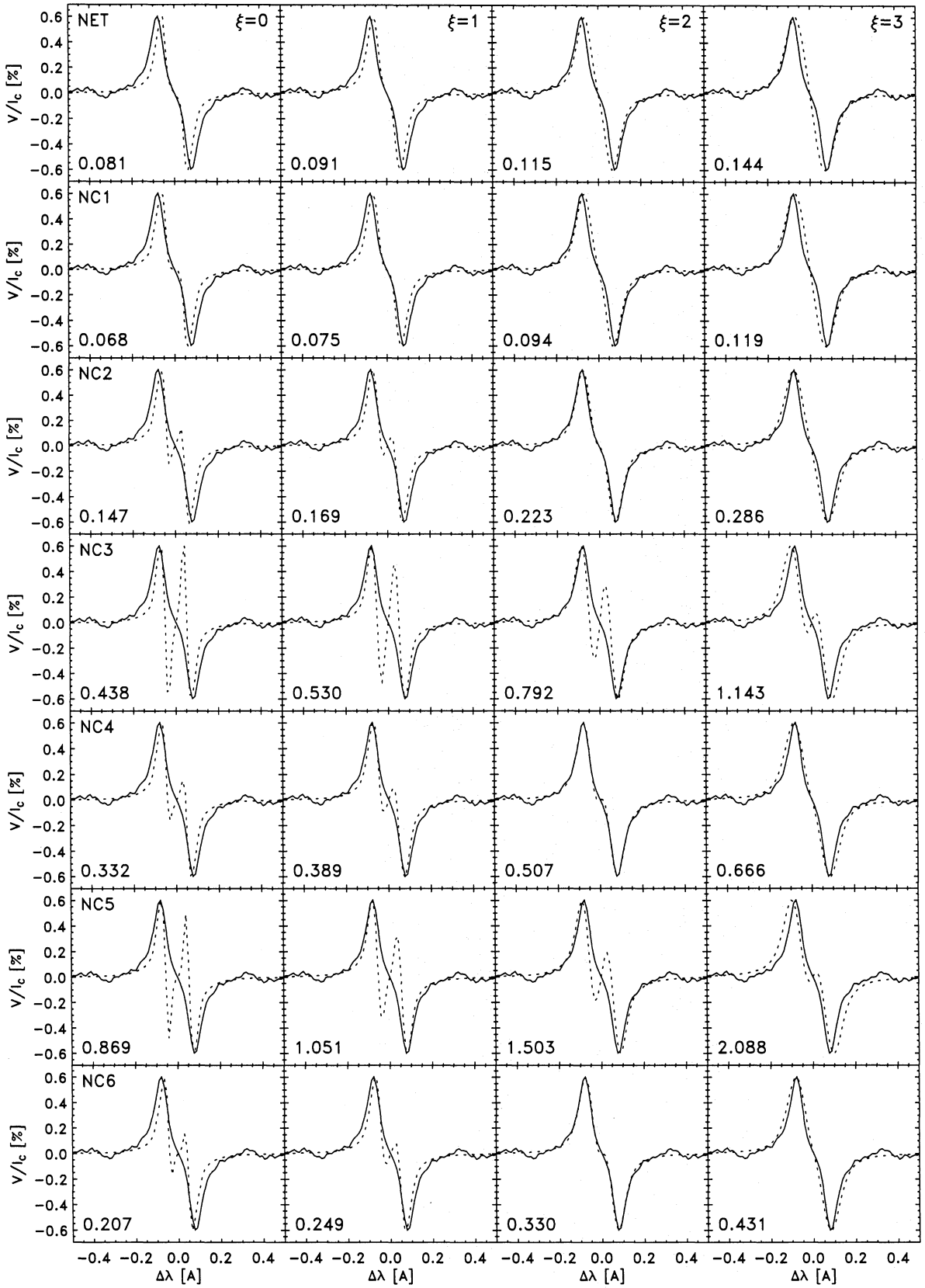

Fig. 8. Stokes V profiles of Fe II 4923.92 Å for seven different network models (rows), with different macroturbulent smearing (columns; velocities specified in upper right corners in top row). Solid curves: anti-symmetrized profiles observed in the network. Dashed curves: synthetic profiles. The Stokes V amplitude scaling factor is indicated in the lower left corner of each panel

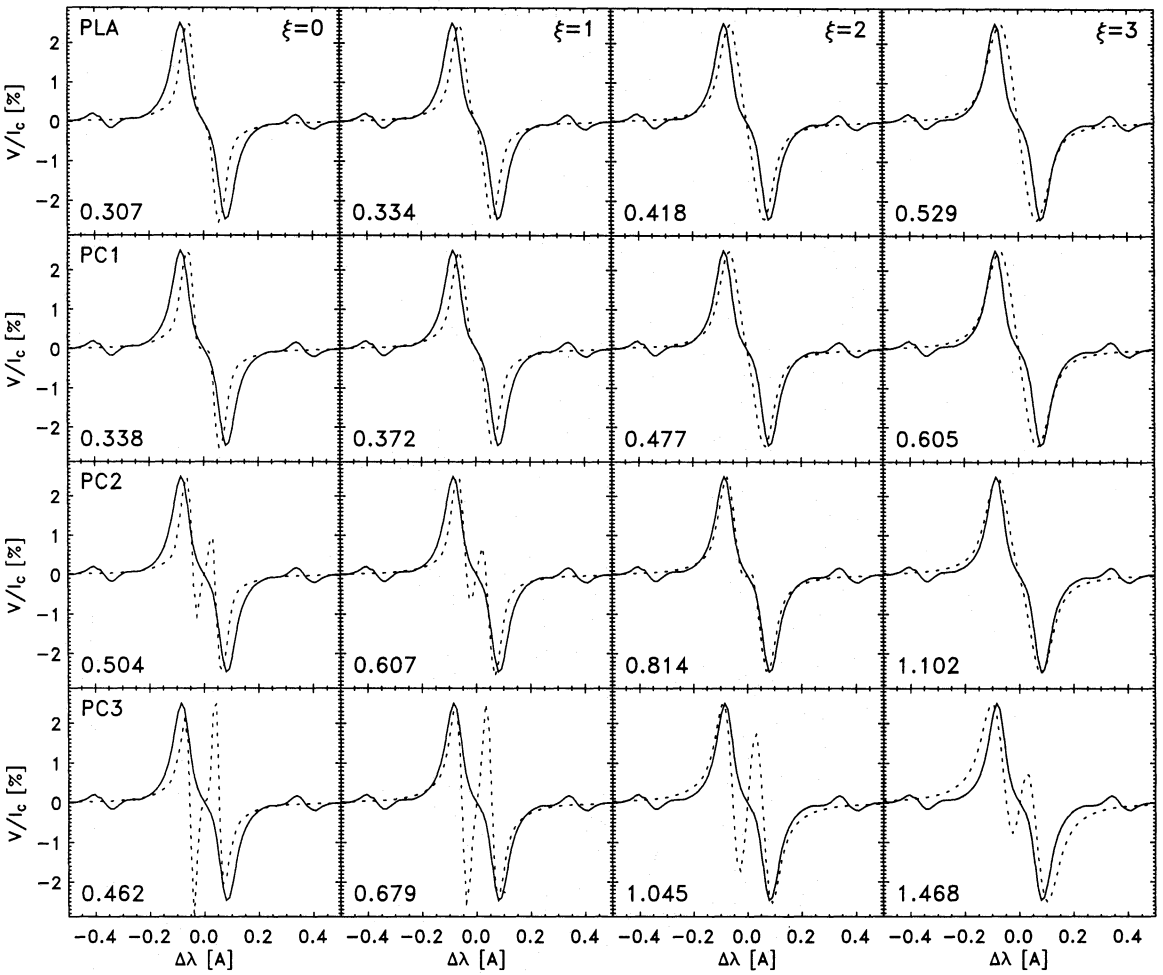

Fig. 9. Dashed curves: Scaled Stokes V profiles of Fe II 4923.92 Å for four different plage models (rows), with different macroturbulent smearing (columns; velocities specified in upper right corners in top row). The Stokes V amplitude scaling factor is indicated in the lower left corner of each panel. Solid curves: anti-symmetrized profiles observed in an active region plage

Table 3. Top part: best-fit macroturbulent velocities (km s^{-1}) determined from amplitude and area scaling factor ratios. Bottom part: Stokes V amplitude scaling factors at the best-fit macroturbulence. The scaling factor averages and their (relative) standard deviations do not include line Fe II 4923.92 Å because of its line center inversions. Due to the problems with fitting Fe I 5405.77 Å this line has been left out completely

λ [Å]	NET	NC1	NC2	NC3	NC4	NC5	NC6	PLA	PC1	PC2	PC3
5083.337	2.10	2.14	2.11	2.15	2.01	2.07	2.09	1.44	1.43	1.48	1.53
5232.938	2.02	2.11	2.04	2.34	1.91	1.75	2.07	1.93	1.89	2.12	1.77
5217.388	2.18	2.21	2.18	2.29	2.15	2.11	2.19	1.80	1.77	1.92	1.72
5383.370	2.01	2.11	2.05	2.29	2.05	2.09	2.06	1.85	1.80	1.98	1.73
4923.925	1.55	1.58	1.78	1.49	1.82	1.55	1.90	1.32	1.39	1.83	0.41
5197.577	1.74	1.75	1.74	1.95	1.84	1.98	1.77	1.29	1.28	1.39	1.58
5325.554	1.95	1.97	1.94	2.02	1.97	1.94	1.97	1.44	1.43	1.53	1.38
5083.337	0.126	0.102	0.216	0.667	0.501	1.394	0.318	0.387	0.426	0.637	0.617
5232.938	0.097	0.079	0.167	0.520	0.361	0.982	0.239	0.337	0.372	0.548	0.521
5217.388	0.108	0.088	0.186	0.557	0.393	0.983	0.265	0.369	0.407	0.602	0.534
5383.370	0.107	0.088	0.187	0.561	0.392	0.990	0.264	0.385	0.426	0.621	0.563
4923.925	0.104	0.086	0.211	0.658	0.486	1.301	0.321	0.360	0.413	0.778	0.550
5197.577	0.087	0.070	0.152	0.503	0.330	0.936	0.218	0.318	0.349	0.530	0.581
5325.554	0.103	0.083	0.175	0.527	0.346	0.820	0.249	0.419	0.457	0.697	0.559
Average	0.105	0.085	0.181	0.556	0.387	1.017	0.259	0.369	0.406	0.606	0.563
Stand. dev.	0.012	0.010	0.020	0.054	0.056	0.178	0.031	0.034	0.036	0.056	0.031
Rel. SD	0.114	0.117	0.111	0.096	0.144	0.175	0.120	0.091	0.088	0.092	0.056

Table 4. Computed Stokes V area ratios for complete set of line pairs, normalized by observed area ratios. Values are for macroturbulence of 2 km s^{-1}

λ line pair	NET	NC1	NC2	NC3	NC4	NC5	NC6	PLA	PC1	PC2	PC3
5083.34 / 5232.94	0.79	0.79	0.79	0.79	0.72	0.72	0.76	0.83	0.84	0.82	0.82
5083.34 / 5217.39	0.85	0.86	0.85	0.82	0.77	0.70	0.82	0.93	0.93	0.91	0.86
5083.34 / 5383.37	0.87	0.88	0.88	0.84	0.78	0.71	0.84	0.96	0.97	0.94	0.90
5083.34 / 4923.92	0.85	0.87	1.01	1.16	0.99	1.02	1.03	0.91	0.94	1.20	1.24
5083.34 / 5197.58	0.71	0.71	0.73	0.78	0.67	0.68	0.71	0.83	0.83	0.84	0.93
5083.34 / 5325.55	0.84	0.84	0.83	0.81	0.69	0.60	0.80	1.12	1.11	1.12	0.96
5232.94 / 5217.39	1.08	1.09	1.08	1.04	1.06	0.98	1.08	1.11	1.11	1.12	1.05
5232.94 / 5383.37	1.11	1.11	1.11	1.07	1.08	0.99	1.10	1.15	1.15	1.14	1.09
5232.94 / 4923.92	1.08	1.11	1.28	1.47	1.36	1.43	1.36	1.09	1.12	1.46	1.50
5232.94 / 5197.58	0.91	0.90	0.92	0.99	0.92	0.95	0.93	1.00	0.99	1.02	1.12
5232.94 / 5325.55	1.07	1.06	1.05	1.03	0.96	0.84	1.05	1.34	1.33	1.37	1.16
5217.39 / 5383.37	1.03	1.02	1.03	1.02	1.02	1.02	1.02	1.03	1.04	1.02	1.04
5217.39 / 4923.92	1.00	1.02	1.18	1.41	1.28	1.46	1.26	0.98	1.01	1.31	1.43
5217.39 / 5197.58	0.84	0.83	0.85	0.95	0.87	0.97	0.86	0.90	0.89	0.92	1.08
5217.39 / 5325.55	0.99	0.98	0.97	0.99	0.90	0.86	0.97	1.21	1.19	1.23	1.11
5383.37 / 4923.92	0.98	0.99	1.15	1.38	1.26	1.44	1.23	0.95	0.97	1.28	1.38
5383.37 / 5197.58	0.82	0.81	0.83	0.93	0.85	0.96	0.84	0.87	0.86	0.89	1.03
5383.37 / 5325.55	0.96	0.96	0.95	0.97	0.89	0.84	0.95	1.17	1.15	1.20	1.07
4923.92 / 5197.58	0.84	0.82	0.72	0.67	0.68	0.67	0.68	0.92	0.89	0.70	0.75
4923.92 / 5325.55	0.99	0.96	0.83	0.70	0.70	0.59	0.77	1.24	1.19	0.94	0.78
5197.58 / 5325.55	1.18	1.18	1.14	1.04	1.04	0.88	1.13	1.34	1.34	1.34	1.04
Average	0.94	0.94	0.96	0.99	0.93	0.92	0.96	1.04	1.04	1.08	1.06
Stand. dev.	0.12	0.12	0.15	0.21	0.20	0.25	0.18	0.15	0.15	0.20	0.20
Rel. SD	0.13	0.13	0.16	0.22	0.21	0.27	0.19	0.15	0.14	0.19	0.18

observed profiles. We stress, however, that this procedure leaves other aspects of the line profiles, such as the widths of the σ-components and, in particular, the gradient $dV/d\lambda$ at line center practically unchanged.

The computed profiles were smeared with a 2 km s^{-1} macroturbulence, which gives acceptable fits to the intensity profiles of all lines. Subsequently they were scaled in Stokes V amplitude and separately in Stokes V profile area (i.e. the area of the absolute value of the Stokes V signal) to fit the observed Stokes V profiles. These Stokes V scaling factors are free parameters, corresponding to changes of the filling factor α of the magnetic part of the model. The scaling factors should be equal for all lines because of magnetic flux conservation. Their variation therefore provides a means of discriminating between flux-tube models. The computed profiles are plotted for the NET model (Fig. 6) and PLA model (Fig. 7) only. For most lines these scaled profiles have approximately the same shape for all models.

Since the Stokes V area and amplitude scaling factors have different dependences on the macroturbulence, for well-behaved V profiles (without line center inversions) a macroturbulence value can be derived for which their ratio is unity. This procedure selects profiles with correct amplitude and area, but, depending on the model, not necessarily the correct line shape. Table 3 lists these best-fit macroturbulent velocities and the interpolated amplitude scaling factors at those velocities for all models.

The Fe II 4923.92 Å line shows by far the largest variation in shape from model to model. In particular, it shows inversions of the line core for almost all models with a chromospheric temperature rise, as long as the macroturbulent velocity $\xi = 0$. Since these inversions have large diagnostic interest Figs. 8 and 9 display the full set of Stokes V profiles for Fe II 4923.92 Å, for the network and plage models, respectively. Note the large influence of ξ on the inversion in the line core: only for 3 models (NC3, NC5 and PC3) does an inversion persist for a macroturbulence of 2 km s^{-1}, which, according to Table 3 is closest to the "best-fit" macroturbulence. However, for the other models that produce an inversion at $\xi = 0$ the profile shape is distinctly different from the profile shape for models without an inversion, even after the inversion has been smeared out by the macroturbulence. The line center inversions make the area scaling factors of Fe II 4923.92 Å erratical, so that this line was excluded from the averages in Table 3.

The Fe I 5405.77 Å line also produces a distinct inversion, but due to the difficulty of fitting its observed quiet-Sun profile, we have not used its V profile for diagnostic purposes. It has been excluded from Tables 3 and 4 for the same reason.

Stokes V area ratios of well-chosen line pairs may reveal trends that are not clear from separate scaling factors. Of particular interest are pairs of lines of different strength, excitation energy, or ionization stage. Table 4 lists these ratios for all models, with 2 km s^{-1} macroturbulent smearing. There is obvious redundancy in this list, since only a set of less than eight ratios can be independent for a set of eight lines.

4. Discussion

Various techniques have been employed to disentangle the magnetic and thermodynamic properties coded into the emergent Stokes I and V profiles. Examples are diagnostics based on Stokes V such as line ratios, presence or absence of line center inversions, line widths, asymmetries, and the zero-crossing wavelength (e.g. Solanki & Stenflo 1984, 1985, Stenflo 1973, 1975, Solanki 1986, Lites et al. 1987). Line shapes, amplitude scaling factors and line area ratios are used here to evaluate the chromospheric models.

From Figs. 4 and 5 it is clear that only Fe II 4923.92 Å, which is the highest-formed line in our sample, is really sensitive to the temperature structure of the lower chromosphere, and to this region alone. The profile shape of Fe II 4923.92 Å (Figs. 8 and 9) indeed responds strongly to chromospheric model changes. All the other lines, when smeared with realistic macrotubulence, have uniform Stokes V profiles over the range of model atmospheres, which renders their profile shapes useless for diagnostic purposes. However, their Stokes V amplitude scaling factors and line area ratios provide additional information.

4.1. Stokes V profiles

The presence of Fe II 4923.92 Å line center inversions for models NC3 and NC5 (Fig. 8) for macroturbulent velocities up to 3 km s^{-1} allows us to discard these modules; they have too high temperatures near $\log \tau_{5000} = -4$. Macroturbulent velocities above 3 km s^{-1} would remove the inversions, but result in too wide profiles. Models NET and NC1 do not cause sufficient inversion in the $\xi = 0$ column of Fig. 8, so that the change in $dV/d\lambda$ near zero-crossing ("inflection" point) is absent in the more realistic $\xi = 2$ column. Indeed none of the models does satisfactorily reproduce the observed Fe II 4923.92 Å profile. This indicates that a chromosphere is present and that it starts lower than in model NC1. The best profile widths are displayed for models NC2, NC4 and NC6 in the $\xi = 2$ column of Fig. 8. These profiles reproduce both the line widths and the observed inflection near zero-crossing. This change in gradient results from the macroturbulent smearing of the line center inversions at left.

For the smaller set of plage models a similar conclusion follows. The presence respectively absence of Fe II 4923.92 Å line center inversions in Fig. 9 demonstrates that temperatures at the line core formation height should be close to PC2, which produces an acceptable Fe II 4923.92 Å line shape, including the $dV/d\lambda$ change near the zero-crossing wavelength.

4.2. Macroturbulence

The synthetic profiles resulting from NET achieve the correct V-profile peak separation only for a macroturbulent velocity larger than 3 km s^{-1}. A similar need for large macroturbulent velocities was noticed by Solanki (1986) and Keller et al. (1990). It appears that some of the macroturbulences required to fit V profiles in LTE may have been overestimated due to the neglect of a chromospheric temperature rise. Our results suggest that all lines studied here may be adequately reproduced with a total turbulent velocity (both micro- and macroturbulence) of 2.0–2.5 km s^{-1}. This is still a sizeable velocity which may have considerable implications for the energy transport in small-scale magnetic features.

4.3. Scaling factors

The interpolated amplitude scaling factors in Table 3 at the best fit macroturbulent velocities yield no clear preference for any chromospheric model. The average scaling factor varies strongly from one model to the other, but the relative standard deviations are comparable.

4.4. Stokes V area ratios

The Stokes V area ratios in Table 4 have to be treated with caution, because they are not all independent. The ratioing removes the necessity to scale the computed Stokes V profiles, but still requires applying macroturbulence; we use 2 km s^{-1} for all lines since that gives the better profile fits. The ratios involving the most sensitive Fe II 4923.92 Å line quite strongly deviate from unity for all models. Unfortunately, this leaves very little options to form ratios between lines of different excitation energies or strengths. We have considered specific line ratios pertaining to small well-defined height ranges in the atmosphere (Fig. 4), in particular the ratio of Fe I 5083.34 Å and Fe I 5217.39 Å for the deeper part of the temperature minimum region, the ratios of Fe I 5232.94 Å, Fe I 5383.37 Å and Fe I 5197.58 Å for the upper part of the temperature minimum, and the ratio Fe I 4923.92 Å and Fe I 5197.58 Å for the lower chromosphere. Ratios with Fe II 5325.55 Å serve to couple the chromospheric temperatures to the photospheric flux-tube temperatures. On the basis of these ratios we cannot select one of the present models as being the best, because at different heights in the atmosphere, different models give best results. Below $\log \tau_{5000} = -2.5$ the cooler models appear to be best. Near $\log \tau_{5000} = -2.5$ models NC2-4 do about equally well, suggesting that a slight temperature rise above the NET model is appropriate there. In higher layers Fe II 4923.92 Å requires fairly low temperatures to avoid Stokes I core emission or too strong Stokes V inversions. Model NC6 was later added to NC1-5 in an attempt to reconcile these indications. It combines a low-temperature upper photosphere with an early but less steep temperature rise in the chromosphere. Tables 3 and 4 and Fig. 8 show that it fits the observations about as well as NC2 and NC4. This demonstrates that the location of the chromospheric temperature rise and its steepness are exchangeable parameters, i.e. they cannot both be constrained by the spectral diagnostics considered here.

The Stokes V area ratios in Table 4 point in the direction of a plage model that is also a combination of all three chromosphere models. Computations for this model have been omitted since the network results already show that the present set of lines cannot define a unique combination of location and steepness of the temperature rise.

5. Conclusion

We have set limits for the location and initial steepness of the chromospheric temperature rise in small-scale flux tubes. In both network and plage flux tubes the chromosphere starts between $\log \tau_{5000} = -3.5$ and $\log \tau_{5000} = -2.5$. The higher up the chromospheric temperature rise starts, the steeper it must be. The rise definitely starts at a greater optical depth within the flux tube than in the surrounding quiet-Sun model, which corresponds to a smaller geometrical height as well. We estimate that the chromospheric temperature rise starts $200 - 300$ km deeper in the atmosphere within flux tubes than in the average quiet-Sun model of Maltby et al. (1986). The height at which it starts does not appear to differ by more than 50 km between network and plage flux tubes, suggesting that the amount of heating in the lower chromosphere per flux tube is almost independent of magnetic filling factor. The photospheric temperature dip near $\log \tau_{5000} = -1.7$ found in previous empirical models of flux tubes (Solanki 1986, Solanki & Brigljević 1992) cannot be discarded as an artefact of LTE, since several line ratios formed at those depths require such low temperatures in an NLTE analysis as well.

However, the present set of lines is unsuited to define narrow ranges for the location and steepness of the chromospheric temperature rise in flux tubes, because the considered spectral lines do not constrain both parameters simultaneously. More strong lines are needed to narrow down the combination. Unfortunately, most stronger Fe I and Fe II lines are in the ultraviolet, where no Stokes measurements are available.

Acknowledgements. We thank M. Carlsson and G.A. Murphy for kindly providing us with their radiative transfer codes, and R.J. Rutten for critically reading the manuscript.

References

Assousa, G. E., Smith, W. H. 1972, ApJ, 176, 259
Ayres, T. R., Testerman, L. 1981, ApJ, 245, 1124
Ayres, T. R., Testerman, L., Brault, J. W. 1986, ApJ, 304, 542
Bruls, J. H. M. J., Rutten, R. J. 1992, A&A, 265, 257
Carlsson, M. 1986, A Computer Program for Solving Multi-Level Non-LTE Radiative Transfer Problems in Moving or Static Atmospheres, Report No. 33, Uppsala Astronomical Observatory
Chapman, G. A. 1981, in F. O. Orrall (ed.), Solar Active Regions, Colorado Univ. Press, Boulder, 43
Corliss, C. H., Tech, J. L. 1967, J. of Research of the NBS, 71A, No. 6, 567
Defouw, R. J. 1976, ApJ, 209, 266
Fuhr, J. R., Martin, G. A., Wiese, W. L. 1988, J. Phys. Chem. Ref. Data, 17, Suppl. 4
Gigas, D. 1986, A&A, 165, 170
Holweger, H., Müller, E. A. 1974, Solar Phys., 39, 19
Jones, H. P., Skumanich, A. 1980, ApJS, 42, 221
Keller, C. U., Solanki, S. K., Steiner, O., Stenflo, J. O. 1990, A&A, 233, 583
Klose, J. Z. 1971, ApJ, 165, 637
Lites, B. W., Skumanich, A., Rees, D. E., Murphy, G. A., Carlsson, M. 1987, ApJ, 318, 930
Maltby, P., Avrett, E. H., Carlsson, M., Kjeldseth-Moe, O., Kurucz, R. L., Loeser, R. 1986, ApJ, 306, 284
Mihalas, D., Auer, L. H., Mihalas, B. R. 1978, ApJ, 220, 1001
Murphy, G. A. 1990, The Synthesis and Inversion of Stokes Spectral Profiles, NCAR Cooperative Thesis No. 124, High Altitude Observatory, Boulder
Murphy, G. A., Rees, D. E. 1990, Operation of the Stokes Profile Synthesis Routine, NCAR Technical Note NCAR/TN-348+IA, High Altitude Observatory, Boulder
Nordlund, Å. 1984, in S. L. Keil (ed.), Small-Scale Dynamical Processes in Quiet Stellar Atmospheres, National Solar Observatory Summer Conference, Sacramento Peak Observatory, Sunspot, p. 181
Nordlund, Å. 1991, in L. Crivellari, I. Hubeny, D. G. Hummer (eds.), Stellar Atmospheres: Beyond Classical Models, NATO ASI Series C-341, KLuwer, Dordrecht, p. 61
Owocki, S. P., Auer, L. H. 1980, ApJ, 241, 448
Rees, D. E. 1969, Solar Phys., 10, 268
Rees, D. E., Murphy, G. A., Durrant, C. J. 1989, ApJ, 339, 1093
Rutten, R. J. 1988, in R. Viotti, A. Vittone, M. Friedjung (eds.), Physics of Formation of FeII Lines Outside LTE, IAU Colloquium 94, Reidel, Dordrecht, p. 185
Schrijver, C. J., Dobson, A. K., Radick, R. R. 1989, ApJ, 341, 1035
Schüssler, M. 1986, in W. Deinzer, M. Knölker, H. H. Voigt (eds.), Small Scale Magnetic Flux Concentrations in the Solar Photosphere, Abhandl. Akad. Wiss. Göttingen, Math.-Phys. Klasse Dritte Folge Nr. 38, Vandenhoeck und Ruprecht, Göttingen, 103
Simmons, G. J., Blackwell, D. E. 1982, A&A, 112, 209
Solanki, S., Steiner, O., Uitenbroek, H. 1991, A&A, 250, 220
Solanki, S. K. 1986, A&A, 168, 311
Solanki, S. K. 1990, in J. O. Stenflo (ed.), The Solar Photosphere: Structure, Convection and Magnetic Fields, Proceedings IAU Symposium 138 (Kiev), Kluwer, Dordrecht, p. 103
Solanki, S. K., Brigljević, V. 1992, A&A, in press
Solanki, S. K., Roberts, B. 1992, MNRAS, 256, 13
Solanki, S. K., Steenbock, W. 1988, A&A, 189, 243
Solanki, S. K., Steiner, O. 1990, A&A, 234, 519
Solanki, S. K., Stenflo, J. O. 1984, A&A, 140, 185
Solanki, S. K., Stenflo, J. O. 1985, A&A, 148, 123
Steiner, O., Pizzo, V. J. 1989, A&A, 211, 447
Stenflo, J. O. 1973, Solar Phys., 32, 41
Stenflo, J. O. 1975, Solar Phys., 42, 79
Stenflo, J. O., Harvey, J. W., Brault, J. W., Solanki, S. 1984, A&A, 131, 333
Stenholm, L. G., Stenflo, J. O. 1977, A&A, 58, 273
Stenholm, L. G., Stenflo, J. O. 1978, A&A, 67, 33
Thévenin, F. 1989, A&AS, 77, 137
Unsöld, A. 1955, Physik der Sternatmosphären, 2nd edition, Springer, Berlin
Vernazza, J. E., Avrett, E. H., Loeser, R. 1981, ApJS, 45, 635
Walton, S. R. 1987, ApJ, 312, 909
Watanabe, T., Steenbock, W. 1986, A&A, 165, 163

This article was processed by the author using Springer-Verlag LaTeX A&A style file version 3.